Image segmentation for velocity model construction and updating

Adam Halpert and Robert G. Clapp

ABSTRACT

Image segmentation can automatically delineate salt bodies in seismic data, an otherwise human-intensive and time-consuming task. In many instances, current segmentation algorithms successfully pick salt boundaries; a logical extension of such work is to apply these methods to the task of building and updating seismic velocity models. We apply image segmentation tools in conjunction with sediment- and salt-flood velocity estimation techniques to identify the top and base of a salt body. Furthermore, previously existing velocity models may be updated based on the results of segmentation and automated boundary picking. By using the existing model as a priori information for the picking algorithm in areas where the segmentation is ambiguous, we calculate an optimized boundary path across a seismic image. For both synthetic and real seismic data, migrations with velocity models derived from this method produce greatly improved images.

INTRODUCTION

The purpose of image segmentation is to automatically divide an image into sections based on specific attributes. Because of its global optimization properties, Normalized Cuts Image Segmentation (Shi and Malik, 2000), or NCIS, is one algorithm with a variety of potential applications to seismic interpretation. The NCIS method was first applied to seismic data by Hale and Emanuel (2002, 2003) to paint 3D atomic meshes of seismic images. Recent work (Lomask, 2007; Lomask et al., 2007) presents an image segmentation algorithm for automatic picking of salt boundaries on migrated seismic images. Such a scheme offers many potential benefits for the seismic velocity model building process. In this paper, we adapt Lomask's methods for use in iterative velocity model construction and updating.

A reasonably accurate velocity model is an essential component of the seismic imaging process. Much of today's seismic data is acquired in regions with complex salt bodies; in such cases, clearly delineating salt interfaces is often one of the most human-intensive, time consuming and ambiguous aspects of velocity estimation. Accurate salt interface interpretation becomes especially important when the imaging target is located beneath a salt body, as is often the case for modern surveys. The method we propose here is designed to function as a tool for either velocity model

construction or updating. We show our method to be highly effective when combined with widely used sediment- and salt-flooding migration techniques to make original salt interface interpretations. A current limitation of the segmentation algorithm is its ability to handle uncertainties along the boundary path; the same picking rules are imposed throughout the image, even if some areas would benefit from using different rules. Therefore, we also propose a means of producing an improved boundary path by solving a global, non-linear optimization problem. We employ this optimized boundary to update an existing velocity model, so the optimization scheme incorporates the original model as prior information about the boundary in areas of uncertainty. We show both real and synthetic data examples of this method producing an improved velocity model.

THEORY

The segmentation algorithm we use (Lomask, 2007; Lomask et al., 2007) divides a seismic image into two segments, salt and sediment; the boundary separating them is the salt interface. The segmentation is based on a specific seismic attribute, in most cases amplitude of the envelope, that can clearly differentiate between a salt body and the surrounding sediments. The first step is to create a weight matrix, $\mathbf{W}$, relating each pixel in a migrated seismic image to a collection of neighboring pixels. Thus, $\mathbf{W}$ is necessarily many times larger than the input image, although Lomask (2007) describes several methods to improve computational efficiency. One such method is to assign weights for only a random sampling of neighbors for each pixel, rather than all pixels within a given distance. The weight associated with a pair of pixels is inversely proportional to the maximum value of the envelope along the shortest path connecting those two pixels, multiplied by a distance weighting term. Thus, low weights are assigned to pixel pairs most likely to be separated by a salt boundary. Subject to constraints, the path across the image minimizing the sum of the weights through which it passes is the salt boundary.

Following the NCIS algorithm of Shi and Malik (2000), Lomask showed that the determination of a boundary path across a seismic image may be set up as an eigenvector problem via the Rayleigh quotient

$$\min_{\mathbf{y}} \frac{\mathbf{y^T}(\mathbf{D}-\mathbf{W})\mathbf{y}}{\mathbf{y^T}\mathbf{D}\mathbf{y}} \ , \tag{1}$$

where $\mathbf{y}$ is the eigenvector and $\mathbf{D}$ is a diagonal matrix whose elements are the sum of each column of $\mathbf{W}$. Because of constraints introduced on the Rayleigh quotient, it will be minimized by the eigenvector corresponding to the second smallest eigenvalue of the eigensystem

$$(\mathbf{D}-\mathbf{W})\mathbf{y} = \lambda\mathbf{D}\mathbf{y} \ , \tag{2}$$

where λ is the eigenvalue. The eigenvector $\mathbf{y}$ will have values ranging from -1 to 1 across the boundary; in most cases, following the "zero contour" across the image yields the most appropriate salt interface pick. When the zero contour is not clearly

defined (see Figure 1), it may be necessary to use another value of the eigenvector to pick the boundary. The determination of this value in different parts of the image can be posed as an optimization problem, and is discussed later.

A note about migration

Because segmentation operates on migrated data, the success of this method is highly dependent on the migration algorithms used and the quality of the resulting images. For the examples in this paper, we elected to use plane wave migration in tilted Cartesian coordinates (Shan and Biondi, 2007; Shan, 2008). Figure 1 shows eigenvectors calculated for the same section of a Gulf of Mexico dataset. The eigenvector in (a), taken from Lomask (2007), is derived from an image obtained with a one-way wave-equation method; for (b), the image used is obtained through Shan's plane wave migration. The eigenvector in (b) is clearly superior, as the transition from positive to negative values (white to black) is sharp for more of the image than on the left. This implies reduced uncertainty in the boundary pick.

Migration in tilted coordinates also achieves better results than plane wave migration in conventional coordinates. Figure 2 displays a portion of the Sigsbee dataset that will be used throughout this paper. Both images in the top row are obtained through plane wave migration with a perfect velocity model, either in a regular coordinate system (a), or with tilted coordinates (b). The right-hand image is superior, most noticeably along the steeply dipping walls of the salt canyon. The corresponding eigenvectors, shown in (c) and (d), again feature less path uncertainty for the eigenvector derived from the superior image.

VELOCITY MODEL CONSTRUCTION

A typical procedure for locating salt boundaries in seismic data is to perform migrations using "flood" velocity models. First, migrate strictly with sediment velocities throughout the entire section; theoretically, the top salt interface will be well resolved. A second migration with salt velocities flooded below the top boundary pick resolves the base of the salt body. In both cases, manually picking the salt boundaries can be time-consuming and inexact, especially for salt bodies with complex geometries. Here, we show that image segmentation can greatly expedite this process.

For this example we use a portion of the Sigsbee 2a synthetic dataset, shown in Figure 2 after migration with a perfect velocity model. Figure 3 shows the result of migration with a sediment-flooded velocity model, created by infilling the salt portions of the Sigsbee model with sediment velocities. Much of the top salt interface is extremely well resolved and relatively easy to pick; however, the boundary disappears inside the salt canyon, and would be difficult to pick manually. The top row of Figure 4 illustrates the image segmentation process: (a) is the eigenvector calculated for the image, and (b) is the boundary pick corresponding to the zero contour of the

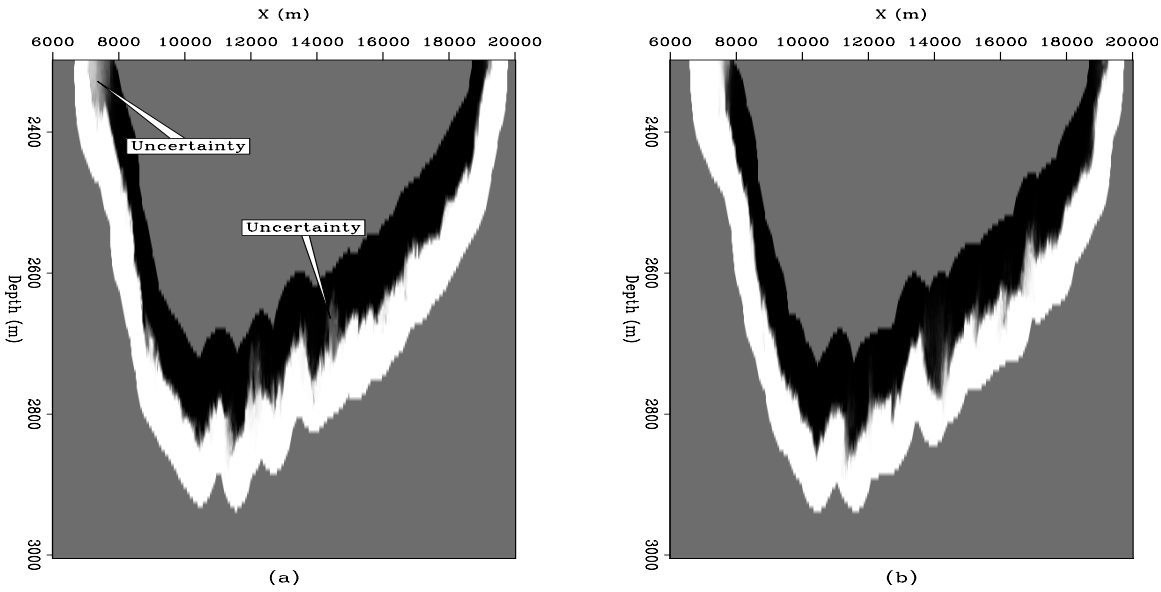

Figure 1: Eigenvectors derived from images obtained through two different migration algorithms: a conventional downward continuation method (a), and plane wave migration in tilted coordinates (b). [**CR**]

eigenvector. The method accurately picks the complex geometry along the top of the salt, and correctly interprets the presence of the canyon.

One way to measure the quality of the method's top boundary pick is to observe the quality of a salt flood migration using a velocity model derived from the top boundary pick. Figure 4c shows the eigenvector resulting from an image migrated with salt velocities flooded below the top boundary pick. There is little to no uncertainty along the zero contour. As expected, the base salt reflection in image (d) is strong and clear throughout the image; the overlain boundary confirms that the segmentation algorithm tracks the interface well.

VELOCITY MODEL UPDATES

Image segmentation may also be used as a tool in an iterative boundary-picking process to update a previously existing velocity model or salt body interpretation. For this task, such a preexisting model offers a potential advantage over picking a boundary without any prior information, as was the case for the sediment- and salt-flood models. Namely, the existing model can act either as a guide or a penalty for the boundary-picking algorithm in areas where the appropriate boundary choice is not obvious.

Uncertainty in the method's salt interface pick arises when the eigenvector transitions smoothly from negative to positive values. These areas of uncertainty appear gray on depictions of the eigenvector such as Figure 1, rather than sharp transitions

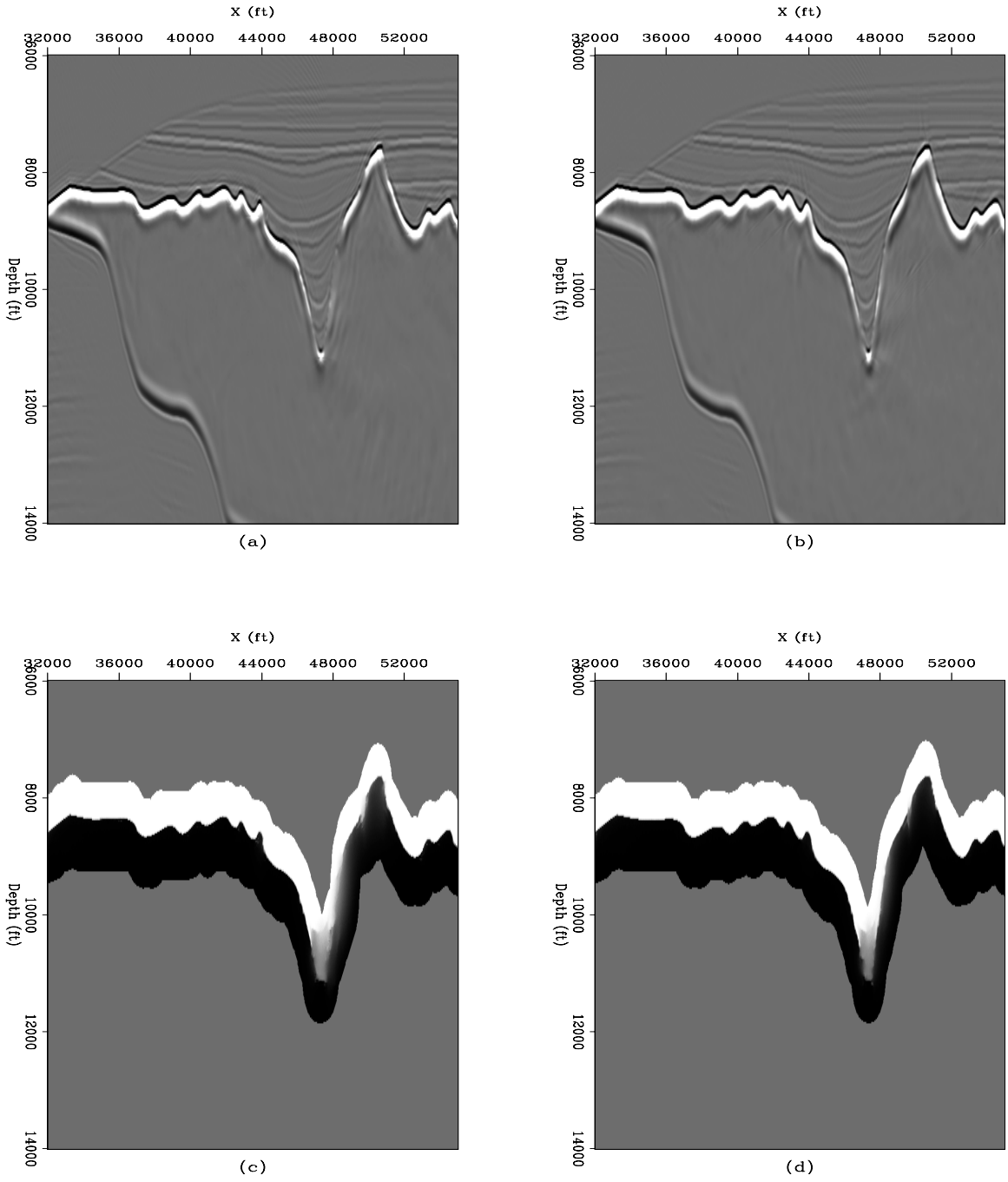

Figure 2: Top: A section of the Sigsbee synthetic model imaged using plane wave migration in (a) a regular coordinate system and (b) tilted Cartesian coordinates. Bottom: Eigenvectors corresponding to the images directly above. Note both the improved imaging of the salt canyon walls, as well as the reduced eigenvector path uncertainty when tilted coordinates are used. [**CR**]

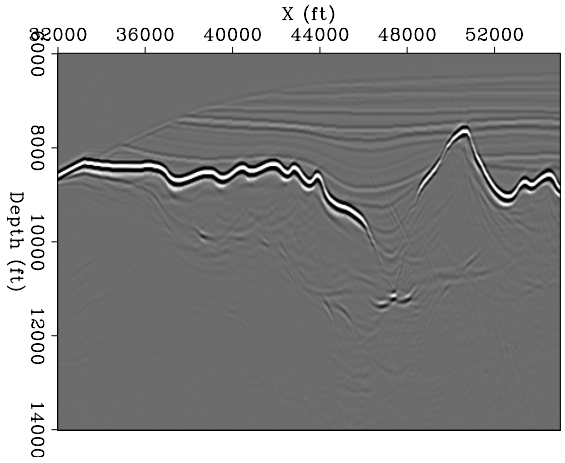

Figure 3: A sediment flood migration of the Sigsbee data. Most of the top salt boundary is well resolved, but the details of the salt canyon are highly ambiguous. [**CR**]

from black to white indicative of a relatively certain boundary pick. In a given area of uncertainty, the boundary pick may be improved by manually selecting a non-zero eigenvector contour value to follow throughout the image. However, Lomask (2007) notes that any such improvement in one part of the image may be "matched by a reduction of picking quality in other uncertain areas." Thus, a natural extension of Lomask's work is to pose the boundary picking task as a global optimization problem, in which the boundary is allowed to follow different contour values throughout the image.

Optimizing the boundary

We set up a non-linear inverse problem that attempts to find the optimal depth for the salt-sediment interface at each $\mathbf{x}$ position in the image. Currently, a limitation of this method is the inability to handle boundaries that are not single-valued functions of $\mathbf{x}$.

1. In most cases, the eigenvector's zero contour is the most appropriate path. Therefore, a primary fitting goal should seek to follow the zero contour wherever possible. This goal results in a non-linear system; we cannot create a linear system that maps between reflector depth and the eigenvector. As a result, we must create a linear operator, $\mathbf{G}$, by linearizing the problem around the zero-contour boundary $\mathbf{m}_0$. First, we calculate the depth gradient at each point for every trace in the eigenvector. The operator $\mathbf{G}$ is then formed by extracting the gradient value at each point along the zero-contour boundary $\mathbf{m}_0$. In equation 3 below, the deviation $\mathbf{\Delta m}$ from the zero-contour boundary is very small when $\mathbf{G}$ is large (high certainty), and larger when $\mathbf{G}$ is small (uncertainty).

2. The zero contour may be inappropriate in areas of great uncertainty. Here, it is beneficial to rely more upon the a priori information - a previous boundary ($\mathbf{m}_{\text{orig}}$) manually suggested by an experienced interpreter, or the results of the

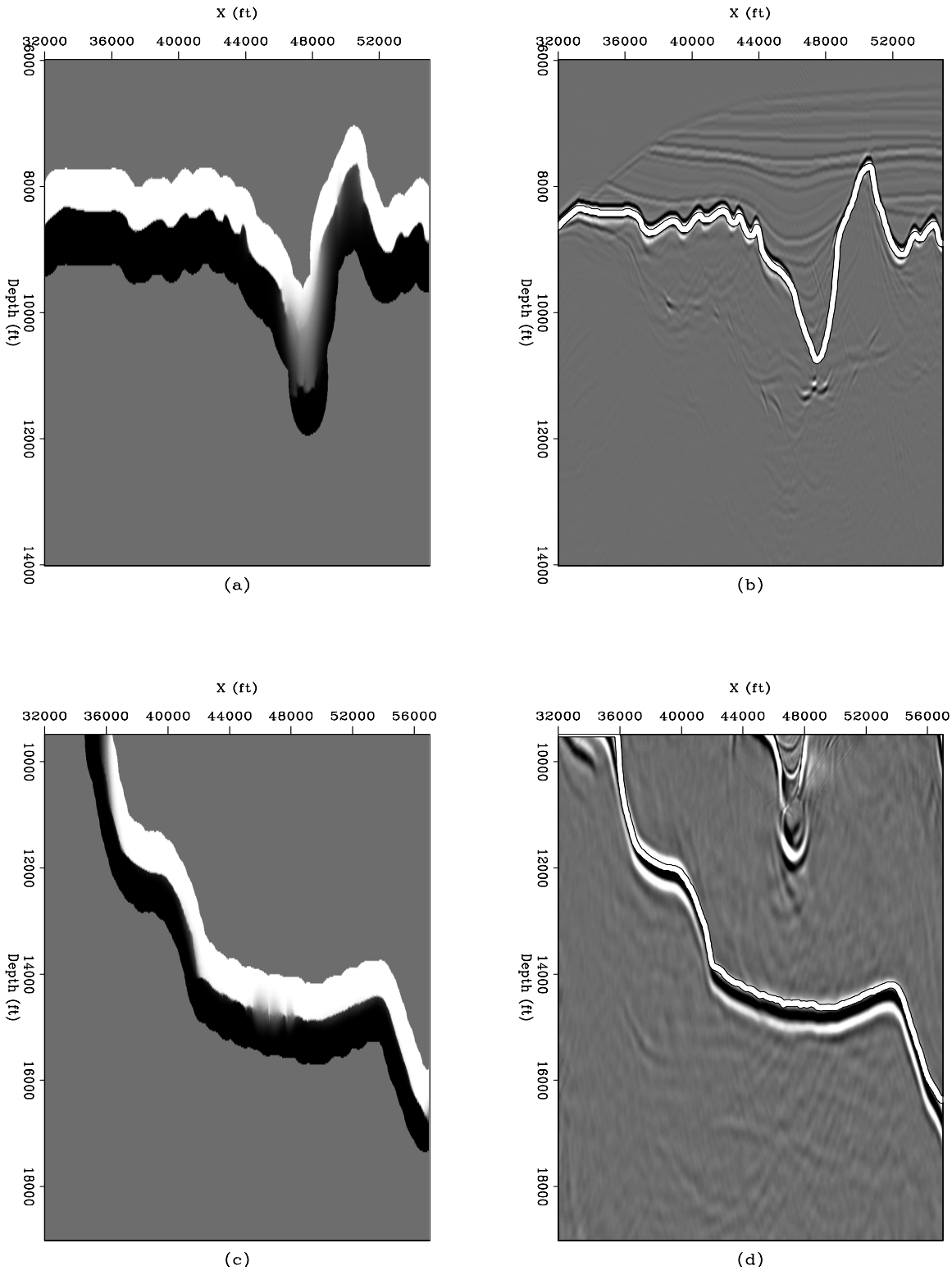

Figure 4: Top: Eigenvector (a) and picked boundary (b) from a sediment-flood migration of the Sigsbee data. Bottom: Eigenvector (c) and picked boundary (d) for the base of the Sigsbee salt body after a salt-flood migration. [**CR**]

flood migration procedure detailed above. In the former case, the prior boundary can act as a guide; the optimized boundary will tend to follow the previous one in uncertain areas. In the latter case, however, it may be obvious that the prior boundary is placed either too deep or too shallow in the model. In this circumstance, the previous boundary may be penalized so that the optimized boundary will move *away* from the previous one rather than toward it. To implement this goal, we construct a diagonal weighting matrix $\mathbf{P}$ such that areas of uncertainty are given greater weights. The weights in $\mathbf{P}$ may have positive or negative values, depending on the need to either penalize or reward the prior boundary.

3. Finally, to avoid unwanted fluctuations in the boundary pick, a smoothing constraint is imposed on the boundary in the form of a 1D gradient roughening operator ($\mathbf{A}$).

Mathematically, the above goals may be expressed as a series of minimization equations:

$$0 \approx \mathbf{G}\ \mathbf{\Delta m} \tag{3}$$

$$0 \approx \mathbf{P}(\mathbf{m} - \mathbf{m}_{\text{orig}}) \tag{4}$$

$$0 \approx \mathbf{A}\mathbf{m}\ . \tag{5}$$

Because the problem posed here is non-linear, we solve it iteratively using the Newton method to implement the above equations and calculate a new boundary model $\mathbf{m}_i$. Defining the previous boundary model as $\mathbf{m}_{i-1}$, and our current model as a function of non-linear iteration j as $\mathbf{m}_i^j$, and two relative weighting parameters ϵ_1 and ϵ_2 we begin with the zero-contour boundary and iterate to convergence using the following scheme:

Iterate over j
{
Construct $\mathbf{L} = [\mathbf{G}\mathbf{m}_i^j \quad \epsilon_1\mathbf{P} \quad \epsilon_2\mathbf{A}]^{\mathrm{T}}$
Calculate current residual $\mathbf{r} = [0 \quad -\mathbf{P}\mathbf{m}_{i-1} \quad 0]^{\mathrm{T}} - \mathbf{L}$
Solve the linear system
$\mathbf{r} = \mathbf{L}\Delta\mathbf{m}_i^j$
$\mathbf{m}_i^j = \mathbf{m}_i^{j-1} + \Delta\mathbf{m}_i^j$
}

For 2D cases on the scale of the examples shown here, the computational expense for this scheme is virtually negligible. A possible future enhancement to the algorithm presented here will be to incorporate residual map migration to remap the original boundary. This would help eliminate bias introduced by movements of the migrated reflectors with respect to the image obtained with the original velocity model.

Velocity model update: Examples

Here, we present updated velocity models for both the section of the Sigsbee synthetic data used previously and a section of the 2D Gulf of Mexico dataset that Lomask (2007) used to demonstrate his segmentation algorithm. Once we calculate an optimum boundary using the procedure detailed above, we generate an updated velocity model based on a comparison with the original velocity model. Any sediment velocities below the picked upper salt boundary are filled with salt velocities, and salt velocities above the boundary pick are replaced with nearby sediment velocities. By remigrating with the updated velocity models, improved images are obtained.

Figure 5 displays a typical sequence for producing an improved image by updating a preexisting velocity model. In this case, the prior boundary model is the salt interface picked after the sediment-flood migration of the Sigsbee data, shown in Figure 4b. It is clear that this boundary places the bottom of the canyon too shallow, as the canyon bottom image is pushed down by the presence of excess salt velocities. Figure 5b confirms that the zero contour boundary would still be picked too shallow at the bottom of the canyon. Therefore, the prior boundary is penalized in the optimization scheme; the optimized boundary will move away from the previous one in uncertain areas (in this case, only the canyon bottom). Figure 5c shows the result of the boundary optimization process - as expected, the bottom of the canyon is now placed deeper in the section. After remigration with a velocity model derived from the new boundary, the resulting image in Figure 5(d) is vastly improved.

In his thesis work, Lomask used a real Gulf of Mexico dataset provided by WesternGeco to demonstrate his segmentation algorithm. Here, we use the optimized boundary/updated velocity model method to produce an improved image. Figure 7 compares the original and updated velocity models used for migration, and Figure 6 shows the results of boundary optimization and remigration. The boundary on the original image is highly discontinuous, and would be difficult to pick either manually or with most horizon tracking algorithms. In this case, it is much more difficult to tell whether the originally interpreted boundary is picked too deep or too shallow; therefore, it is advantageous to use the prior boundary as a guide rather than a negative example. The optimized boundary (Figure 6b) and resulting updated velocity model (Figure 7b) are smoother and feature fewer dramatic changes in the salt interface geometry. After migrating with the updated velocity model, the imaged boundary (Figure 6c) is smoother and more continuous than in the original image.

CONCLUSIONS

Lomask's work on salt body delineation via image segmentation is used in conjunction with plane wave migration in tilted Cartesian coordinates to build and update seismic velocity models. When applied to sediment- and salt-flood migrations of the Sigsbee synthetic dataset, this method provides relatively accurate picks of the top and bottom salt boundaries. These boundaries are used to construct a reasonably

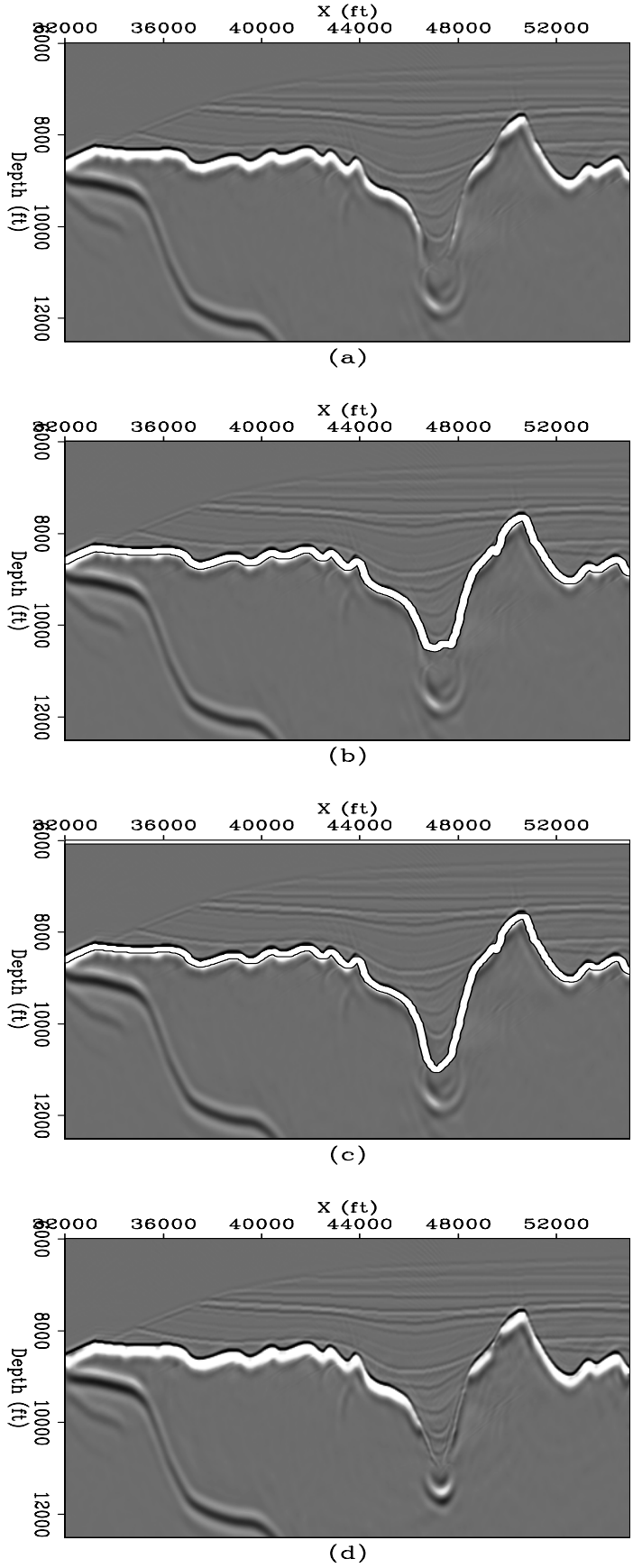

Figure 5: Sequence for using an updated velocity model to produce an improved image. (a) Salt canyon image after migration with the salt-flood velocity model. The original velocity model places the canyon bottom too shallow, pushing the image down. (b) The zero-contour boundary is still clearly too shallow, so the original boundary will be "penalized." (c) Optimized, deeper boundary pick used to create an updated velocity model. (d) A much improved image of the canyon after remigration with the updated velocity. [**CR**]

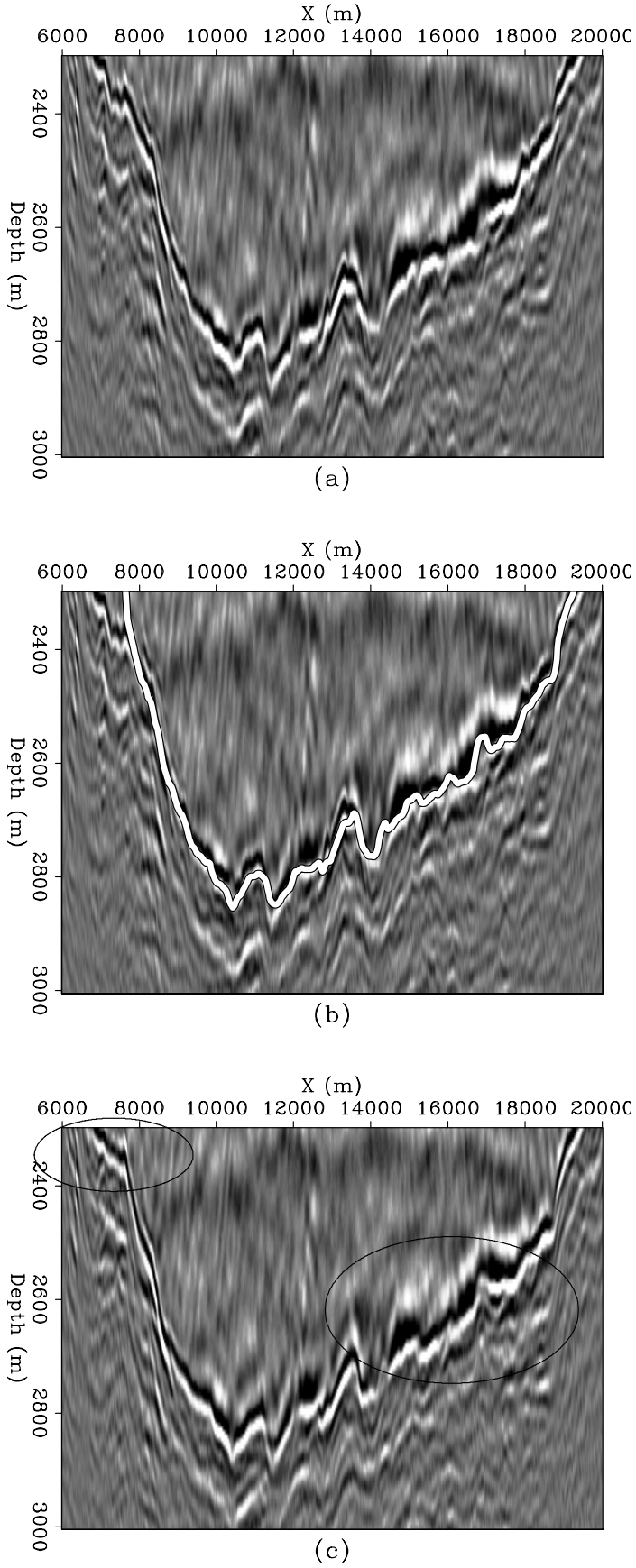

Figure 6: Original image (a), optimized boundary path (b), and updated image (c) for a portion of a Gulf of Mexico dataset. The updated image features a more continuous salt interface than in the original, especially within the indicated areas. [**CR**]

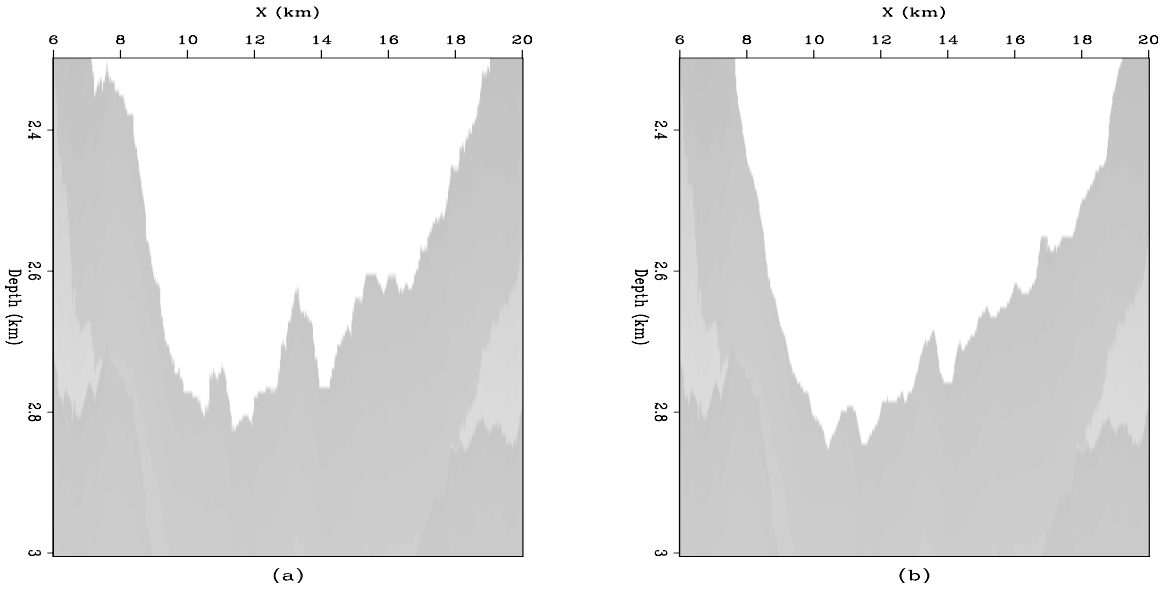

Figure 7: Original (a) and updated (b) velocity models for the section shown in Figure 6. [**ER**]

accurate seismic velocity model. The method is also used to update preexisting velocity models. Since Lomask's method is prone to error in cases where the "best" boundary pick can be produced using different eigenvector contour values in different parts of an image, the boundary choice is posed as an optimization problem. By allowing different contour values to be used throughout the same image, an optimized boundary is calculated. Velocity models derived from the optimized boundary pick produce improved migrated images, both for synthetic and real data.

ACKNOWLEDGMENTS

We would like to thank SMAART JV for the Sigsbee synthetic dataset, and WesternGeco for providing the Gulf of Mexico data.

REFERENCES

Hale, D. and J. U. Emanuel, 2002, Atomic meshing of seismic images, *in* Expanded Abstracts, 2126–2129, SEG.

———, 2003, Seismic interpretation using global image segmentation, *in* Expanded Abstracts, 2410–2413, SEG.

Lomask, J., 2007, Seismic volumetric flattening and segmentation: PhD thesis, Stanford University.

Lomask, J., R. G. Clapp, and B. Biondi, 2007, Application of image segmentation to tracking 3d salt boundaries: Geophysics, **72**, P47–P56.

Shan, G., 2008, Imaging of steep reflectors in anisotropic media by wavefield extrapolation: PhD thesis, Stanford University.

Shan, G. and B. Biondi, 2007, Plane-wave migration in tilted coordinates: SEP-Report, **131**.

Shi, J. and J. Malik, 2000, Normalized cuts and image segmentation: Institute of Electrical and Electronics Engineers Transactions on Pattern Analysis and Machine Intelligence, **22**, 838–905.